PET Imaging and Protein Expression of Prostate-Specific Membrane Antigen in Glioblastoma: A Multicenter Inventory Study

Sanne A.M. van Lith*[1], Ilanah J. Pruis*[2], Nelleke Tolboom[3], Tom J. Snijders[4], Dylan Henssen[1], Mark ter Laan[5], Maarten te Dorsthorst[5], William P.J. Leenders[6,7], Martin Gotthardt[1], James Nagarajah[1], Pierre A. Robe[4], Philip De Witt Hamer[8], Harry Hendrikse[9], Daniela E. Oprea-Lager[9], Maqsood Yaqub[9], Ronald Boellaard[9], Pieter Wesseling[10,11], Rutger K. Balvers[12], Frederik A. Verburg[2], Anita A. Harteveld[2], Marion Smits[2,13], Martin van den Bent[14], Sophie E.M. Veldhuijzen van Zanten*[2], and Elsmarieke van de Giessen*[9]

*[1]Medical Imaging, Radboud University Medical Center, Nijmegen, The Netherlands; [2]Radiology and Nuclear Medicine, Erasmus MC, Rotterdam, The Netherlands; [3]Radiology and Nuclear Medicine, University Medical Center Utrecht, Utrecht, The Netherlands; [4]Neurology and Neurosurgery, UMC Utrecht Brain Center, University Medical Center Utrecht, Utrecht, The Netherlands; [5]Neurosurgery, Radboud University Medical Center, Nijmegen, The Netherlands; [6]Biochemistry, Radboud University Medical Center, Nijmegen, The Netherlands; [7]Predica Diagnostics, Nijmegen, The Netherlands; [8]Neurosurgery, Amsterdam UMC, VUmc, Amsterdam, The Netherlands; [9]Radiology and Nuclear Medicine, Amsterdam UMC, VUmc, Amsterdam, The Netherlands; [10]Pathology, Amsterdam UMC, VUmc, Amsterdam, The Netherlands; [11]Pathology, Princess Máxima Center for Pediatric Oncology, Utrecht, The Netherlands; [12]Neurosurgery, Erasmus MC, Rotterdam, The Netherlands; [13]Medical Delta, Delft, The Netherlands; and [14]Brain Tumor Center at Erasmus MC Cancer Institute, Erasmus MC, Rotterdam, The Netherlands

Upregulation of prostate-specific membrane antigen (PSMA) in neovasculature has been described in glioblastoma multiforme (GBM), whereas vasculature in nonaffected brain shows hardly any expression of PSMA. It is unclear whether PSMA-targeting tracer uptake on PET is based on PSMA-specific binding to neovasculature or aspecific uptake in tumor. Here, we quantified uptake of various PSMA-targeting tracers in GBM and correlated this with PSMA expression in tumor biopsy samples from the same patients. **Methods:** Fourteen patients diagnosed with de novo ($n = 8$) or recurrent ($n = 6$) GBM underwent a preoperative PET scan after injection of 1.5 MBq/kg [^{68}Ga]Ga-PSMA-11 ($n = 7$), 200 MBq of [^{18}F]DCFpyl ($n = 3$), or 200 MBq of [^{18}F]PSMA-1007 ($n = 4$). Uptake in tumor and tumor-to-background ratios, with contralateral nonaffected brain as background, were determined. In a subset of patients, PSMA expression levels from different regions in the tumor tissue samples ($n = 40$), determined using immunohistochemistry ($n = 35$) or RNA sequencing ($n = 13$), were correlated with tracer uptake on PET. **Results:** Moderate to high (SUV_{max}, 1.3–20.0) heterogeneous uptake was found in all tumors irrespective of the tracer type used. Uptake in nonaffected brain was low, resulting in high tumor-to-background ratios (6.1–359.0) calculated by dividing SUV_{max} of tumor by SUV_{max} of background. Immunohistochemistry showed variable PSMA expression on endothelial cells of tumor microvasculature, as well as on dispersed individual cells (of unknown origin), and granular staining of the neuropil. No correlation was found between in vivo uptake and PSMA expression levels (for immunohistochemistry, $r = -0.173$, $P = 0.320$; for RNA, $r = -0.033$, $P = 0.915$). **Conclusion:** Our results indicate the potential use of various PSMA-targeting tracers in GBM. However, we found no correlation between PSMA expression levels on immunohistochemistry and uptake intensity on PET. Whether this may be explained by methodologic reasons, such as the inability to measure functionally active PSMA with immunohistochemistry, tracer pharmacokinetics, or the contribution of a disturbed blood–brain barrier to tracer retention, should still be investigated.

Key Words: glioblastoma; prostate-specific membrane antigen (PSMA); PET; immunohistochemistry; RNA sequencing

J Nucl Med 2023; 64:1526–1531
DOI: 10.2967/jnumed.123.265738

Glioma is the most frequent type of primary brain tumor, of which glioblastoma multiforme (GBM) is the most malignant subtype. Newly diagnosed GBM patients face a dismal prognosis, with a median overall survival time of 15–18 mo. Treatment options are limited, especially at progression. Therefore, research into targeted therapies is highly desired.

A target that has gained increased attention is prostate-specific membrane antigen (PSMA), a type 2 transmembrane glycoprotein receptor that was found to be expressed on neovasculature of various solid tumors (*1*). Immunohistochemistry studies have shown that in GBM, PSMA is expressed on neovasculature in 31%–100% of cases (*2–12*) and absent from vasculature in nonaffected brain areas. High expression of PSMA on neovasculature in GBM correlates with increased angiogenesis (*9*) and poor prognosis (*3,5,8,9*). Besides expression on neovasculature, expression of PSMA has been observed on tumor cells, although to a lesser extent (*8,13*), and tumor cell expression levels did not correlate with survival (*5*).

Various PSMA-targeting radiotracers are used in clinical practice for detection, staging, recurrence evaluation, and radionuclide therapy in prostate cancer (*14*). Some of these tracers have been applied recently to molecular imaging of GBM. These studies showed enhanced uptake of all investigated PSMA-targeting tracers in both de novo and recurrent GBM (*7,15–21*). However, it is unknown whether the current tracers bind specifically to PSMA-expressing

Received Mar. 16, 2023; revision accepted May 31, 2023.
For correspondence or reprints, contact Sophie Veldhuijzen E.M. van Zanten (s.veldhuijzenvanzanten@erasmusmc.nl).
*Contributed equally to this work.
Published online Aug. 31, 2023.

microvasculature or tumor cells or the uptake visible on PET images simply reflects a disturbed blood–brain barrier, resulting in aspecific retention of the tracer. For the potential of PSMA-targeting radionuclide therapy, exact localization of the tracer in the tumor area is considered important, because lack of internalization in tumor cells could lead to rapid washout and short retention times (*22*). Furthermore, particularly for α-emitting radionuclides with high linear energy but short range, internalization into tumor cells—or at least sufficient retention time at the tumor site—would likely be needed to enable effective induction of cellular damage.

In this multicenter inventory study, we aimed to evaluate tumor uptake of several PSMA-targeting tracers ([^{18}F]PSMA-1007, [^{18}F]DCFPyl, and [^{68}Ga]Ga-PSMA-11) in patients with histopathologically confirmed de novo or recurrent GBM. In a subset of patients, we correlated tracer uptake visible on PET images with PSMA expression in image-guided multisector tumor biopsy samples obtained during resection of the tumor.

MATERIALS AND METHODS

Patients

Nine patients with high suspicion of a de novo or recurrent GBM based on MRI were included in separate prospective studies that were performed at Erasmus Medical Center Rotterdam (Erasmus MC, 5 patients; NCT05798273) and Radboud University Medical Center Nijmegen (Radboudumc, 4 patients; NCT04588454). Ethical approval was obtained separately by each of the local institutional review boards. At Amsterdam University Medical Center (Amsterdam UMC, 3 patients) and University Medical Center Utrecht (UMCU, 2 patients), patients with high suspicion of a recurrent GBM were scanned under compassionate use as part of regular clinical care. All patients gave written informed consent for use of their data. Available data were combined for the purpose of this article in a retrospective setting. More details on materials and methods are presented in the supplemental materials (supplemental materials are available at http://jnm.snmjournals.org).

Image Acquisition

All patients underwent PET scanning on injection of 1 of the 3 PSMA-targeting tracers ([^{68}Ga]Ga-PSMA-11, [^{18}F]DCFPyl, or [^{18}F]PSMA-1007) within a range of 1–17 d before surgery or 1–3 mo before surgery for 2 patients who were scanned at UMCU. The image acquisition details are described in Supplemental Table 1.

Image Analysis

SUVs were calculated to enable semiquantitative analysis of tracer uptake in tumor using in-house software. Volumes of interest were automatically drawn around the brain regions that showed high focal uptake. Tumor-to-background ratios were calculated by dividing SUV_{max} of tumor by SUV_{max} of background, as in Kunikowska et al. (*23*), and SUV_{mean} of tumor by SUV_{mean} of background. In addition, the overlaps between gadolinium-based contrast agents enhancing areas of tumor on MRI and tracer uptake on PET were visually assessed by nuclear physicians. SUV_{max} was also assessed for parotid tissue and liver.

Results of the dynamic (Amsterdam UMC, $n = 3$) and sequential (Erasmus MC, $n = 5$) PET scans were used to determine time–activity curves.

Navigation of Biopsy Samples

In 12 of 14 patients, multiple tissue biopsy samples were collected using per-operative neuronavigation (*24*) from tumor areas with low and high tracer uptake on PET to correlate with PSMA expression on immunohistochemistry or as determined with targeted RNA sequencing. Neuronavigation screenshots were used to visually match the corresponding PET frame and volume of interest to the exact biopsy location. In UMCU, only material from the resected tumor was analyzed according to standard clinical care, and no intraoperative biopsy samples were taken.

PSMA Immunohistochemistry

Tissues samples were either snap-frozen ($n = 8$ biopsy samples in 2 patients at Radboudumc) or formalin-fixed and paraffin-embedded ($n = 12$ biopsy samples in 5 patients at Erasmus MC and $n = 15$ biopsy samples in 3 patients at Amsterdam UMC). Tissue sections were immunostained with mouse anti-PSMA (M3620; Dako). The complete biopsy samples were evaluated by an experienced neuropathologist using a visual 5-point scale, which combined both intensity and extent of the staining (0 = none, 1 = limited, 2 = moderate, 3 = high, and 4 = very high) for 3 tissue components that were found to have the highest PSMA expression in all samples: tumor microvasculature (especially in luminal or endothelial cells, rather than abluminal cells or pericytes), individual cells (of unknown nature) in the periphery of the tumor, and neuropil (which showed granular-like staining). The identified individual cells were well organized and located in the transition zone of tumor tissue and preexistent brain tissue. They were therefore not deemed tumor cells, because these showed a disorganized arrangement and no or hardly any PSMA expression. Because of these low PSMA expression levels, tumor cells were not scored. For each biopsy sample, a total immunohistochemistry score was calculated from the sum of the 3 component scores.

Targeted RNA Sequencing

Tissue biopsy samples ($n = 13$ in 4 patients at Radboudumc) were snap-frozen. Targeted RNA sequencing (*25*) was performed to detect PSMA, angiogenesis-related vascular endothelial growth factor receptors 1 and 2, angiopoietin 1, and angiopoietin 2.

Statistical Analyses

Statistical analysis was performed with SPSS version 24.0.0.1 (IBM Corp.) or with GraphPad Prism version 5.0 (GraphPad Software Inc.). PSMA and angiopoietin 1, angiopoietin 2, and vascular endothelial growth factor expression levels in the biopsy samples obtained from immunohistochemistry or RNA expression were correlated with SUV_{max} obtained from 1-cm spheric volumes of interest on PET. Pearson ρ-correlation and Spearman ρ-correlation were used for normally and nonnormally distributed variables, respectively. A P value of less than 0.05 was considered a statistically significant difference.

RESULTS

Uptake of PSMA-Targeting Tracers in GBM

We included 14 patients with histopathologically confirmed de novo GBM ($n = 8$) or recurrent GBM ($n = 6$) (median age, 64 y; interquartile ratio, 54–74 y; $n = 10$ male, 71%; Supplemental Table 2). Tumor uptake values are summarized in Table 1 (all segmentation data are shown in Supplemental Table 3). Figure 1 shows a representative image from each of the centers. Heterogeneous, moderate to high uptake of all PSMA tracers was found in all tumors. SUV_{max} and tumor-to-background ratio (SUV_{max} of tumor divided by SUV_{max} of background) values ranged from 1.3 to 20.0 and 7.5 to 359.0 for [^{68}Ga]Ga-PSMA-11, from 4.5 to 13.1 and 13.6 to 36.5 for [^{18}F]DCFPyl, and from 3.4 to 14.6 and 6.1 to 39.6 for [^{18}F]PSMA-1007, respectively. Uptake in contralateral nonaffected brain was low (SUV_{max}, <0.1–1.6). Overall, the uptake distribution, as seen on PET, showed good visual overlap with the area of gadolinium-based contrast agent enhancement on T1-weighted MRI. However, an inhomogeneous pattern of PET uptake was seen in the areas enhanced by gadolinium-based contrast agents, which did not exactly follow the contrast agent pattern in all cases (Fig. 1).

TABLE 1
Tumor Uptake of Various PSMA-Targeting Tracers

No.	Radioligand	Time after injection (min)	SUV_{max}	SUV_{mean}	$TBR_{max/max}$
1	[^{68}Ga]Ga-PSMA-11	90 (WB)	15.3	4.4	32.6
		165	20.0	4.5	66.7
		240	17.0	4.0	38.6
2	[^{68}Ga]Ga-PSMA-11	90 (WB)	3.6	1.7	359.0
		165	5.9	2.9	295.0
		240	5.8	2.8	35.9
3	[^{68}Ga]Ga-PSMA-11	90 (WB)	7.4	2.5	185.3
		165	9.8	2.6	98.4
		240	10.0	2.8	26.3
4	[^{68}Ga]Ga-PSMA-11	90 (WB)	6.5	3.1	10.3
		165	9.0	3.5	17.3
		240	9.0	3.6	7.5
5	[^{68}Ga]Ga-PSMA-11	90 (WB)	7.3	1.9	66.6
		165	7.7	2.3	29.5
		240	9.0	2.6	64.6
6	[^{18}F]DCFPyl	80	4.5	2.1	21.9
		NA (WB)	NA	NA	NA
		140	6.8	2.9	25.7
7	[^{18}F]DCFPyl	80	5.3	2.1	23.5
		95 (WB)	4.5	2.3	13.6
		140	7.4	2.7	24.4
8	[^{18}F]DCFPyl	80	10.3	4.6	34.8
		95 (WB)	12.6	5.3	29.9
		140	13.1	6.0	36.5
9	[^{68}Ga]Ga-PSMA-11	60	2.2	1.0	72.3
10	[^{68}Ga]Ga-PSMA-11	60	1.3	0.6	10.3
11	[^{18}F]PSMA-1007	120	3.4	1.6	6.1
12	[^{18}F]PSMA-1007	120	8.1	3.4	10.1
13	[^{18}F]PSMA-1007	120	14.6	6.8	39.6
14	[^{18}F]PSMA-1007	120	12.4	4.7	7.8

$TBR_{max/max}$ = SUV_{max} tumor divided by SUV_{max} background; WB = whole body; NA = not available.

Because normal tissue biodistribution patterns are similar for [^{18}F]DCFPyl and [^{68}Ga]Ga-PSMA-11 (*26*), time–activity curves for tracer uptake in the tumors of patients 1–8, covering 0–240 min after injection, are combined in Figure 2A. These time–activity curves demonstrate that there is still an increase in [^{18}F]DCFPyl binding 120 min after injection and gradual flattening of the curve but still slightly increasing [^{68}Ga]Ga-PSMA-11 binding approaching 240 min after injection. A representative perfusion image of the tumor in the first 2 min after injection for [^{18}F]DCFPyl (Fig. 2B) demonstrates that tumor uptake of [^{18}F]DCFPyl at late time points does not follow the perfusion pattern; that is, tumor uptake primarily depends on factors other than perfusion. Time–activity curves normalized for SUV_{mean} of parotid tissue and SUV_{max} of liver are shown in Supplemental Figure 1.

Uptake of PSMA-Targeting Tracers in Nontarget Organs

Uptake in the parotid glands increased gradually on each of the successive scans within patients and showed high variability between patients, irrespective of the type of tracer (Supplemental Table 2; for the SUV_{max} range, [^{68}Ga]Ga-PSMA-11, 10.4–34.7; [^{18}F]DCFPyl, 9.1–45.6; [^{18}F]PSMA-1007, 22.9–43.8). Uptake in the liver was found with SUV_{max} ranging from 7.7 to 12.9 for [^{68}Ga]Ga-PSMA-11 and 6.6 to 6.7 for [^{18}F]DCFPyl (Supplemental Table 2).

Correlation of Tracer Uptake with PSMA Expression

Figures 3A–3D show representative images of PSMA immunohistochemistry of tumor biopsy samples demonstrating PSMA expression on the 3 tissue components. PSMA expression on microvasculature was mainly found within the boundaries of tumor tissue, whereas PSMA-expressing individual cells were generally located in the transition zone of tumor tissue and preexistent brain tissue. A negative correlation was found between tracer uptake visible on the PET images and immunohistochemistry scores for the individual cells ($r = -0.372$, $P = 0.028$), and no significant correlation was found between PET uptake and immunohistochemistry

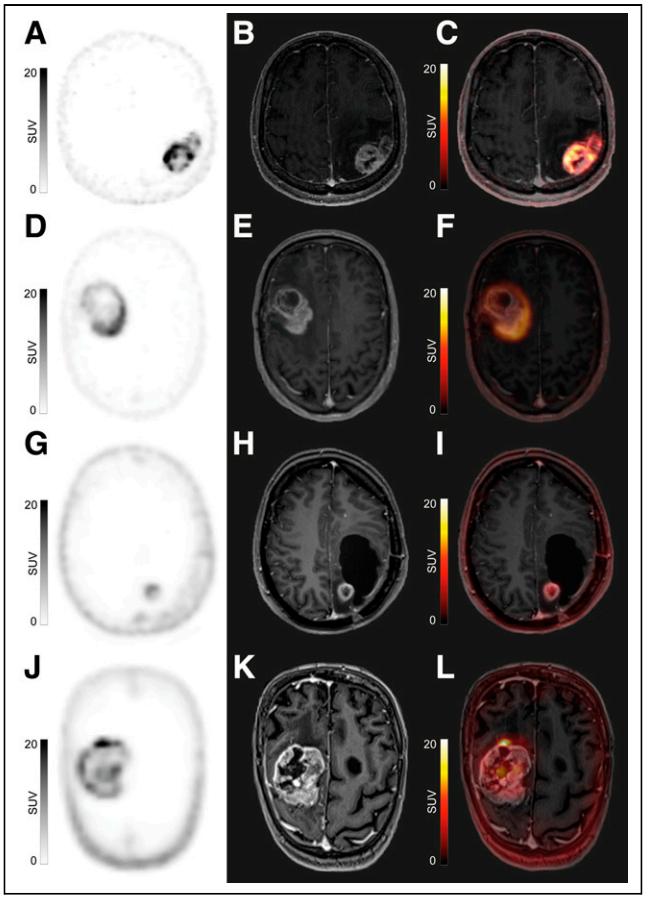

FIGURE 1. Selected examples of PET (A, D, G, and J), MRI (B, E, H, and K), hybrid PET/MRI (C), and fused PET/MRI (F, I, and L) of patients injected with [^{68}Ga]Ga-PSMA-11 (patient 1 from Erasmus MC [A–C], SUV_{max}, 20.0, and patient 10 from UMCU [G–I], SUV_{max}, 1.3), [^{18}F]DCFpyl (patient 8 from Amsterdam UMC [D–F], SUV_{max}, 13.1), and [^{18}F]PSMA-1007 (patient 14 from Radboudumc [J–L], SUV_{max}, 12.4). Note heterogeneity of tracer uptake within tumors.

scores for vasculature ($r = 0.211$, $P = 0.225$), neuropil ($r = -0.077$, $P = 0.660$; Supplemental Fig. 2A), or total immunohistochemistry scores ($r = -0.173$, $P = 0.320$; Fig. 3E). No correlations were found when separated for tracer type (Supplemental Table 4).

No correlation was found between tracer uptake of [^{18}F]PSMA-1007 on PET and PSMA RNA expression ($r = -0.033$, $P = 0.915$; Fig. 3F). PSMA immunohistochemistry and PSMA RNA expression analyses did correlate, confirming the validity of both techniques ($r = 0.773$, $P = 0.029$; Supplemental Fig. 2B). No correlations were found between tracer uptake on PET and RNA expression ratio of angiopoietin 2 to angiopoietin 1 ($r = -0.202$, $P = 0.509$) or vascular endothelial growth factor RNA expression ($r = -0.425$, $P = 0.148$; Supplemental Fig. 2C).

DISCUSSION

Here, we found moderate to high uptake on PSMA PET with heterogeneous distribution in tumor irrespective of tracer type in both de novo and recurrent GBM. No correlation was found between uptake on PSMA PET and PSMA expression, as determined with immunohistochemistry or RNA sequencing.

The reported SUV_{max} and values for SUV_{max} of tumor divided by SUV_{max} of background are comparable to those reported in previous literature (*20,27–29*) and show that variation between tumors is larger than variation between tracers. PSMA immunohistochemistry showed strong staining of microvasculature in the tumor tissue but not in nonaffected brain vasculature or cells, which is in accordance with multiple studies (*6,7,30,31*). The strong granular PSMA staining in neuropil, which is built up from glial cells and neurites or neuronal processes, remains to be unraveled. In addition, the nature of PSMA-positive individual cells, especially in the transition zone of tumor tissue and preexistent brain tissue, awaits further elucidation. On the basis of their morphologic and immunohistochemical characteristics, these cells do not qualify as neoplastic cells or macrophages. These cells possibly are peritumoral single cells related to astrocytosis because of glial fibrillary acidic protein positivity, as found by others (*6,8,32*).

Few earlier studies have shown that PSMA expression correlates with tracer uptake in high-grade glioma (*21*) and other tumor types (*33*). One found a nonsignificant trend ($P > 0.1$) in prostate cancer (*34*). We and others (*35*) did not find a correlation between PSMA expression and tracer uptake. Studies correlating expression levels of other targets, such as L-type amino acid transporters (*36,37*) and somatostatin receptor (*38,39*) with tracer uptake of *O*-(2-[^{18}F]fluoroethyl)-L-tyrosine and [^{68}Ga]Ga-DOTA peptides, respectively, in various types of glioma also found no correlation. This is not surprising given the complex and largely still unknown interplay of in vivo tracer kinetics, (heterogeneous) blood–brain barrier disruption, efflux rates, target localization, tracer–target complex kinetics, and downstream function or actions of the target. In addition, methodologic issues, such as the use of different tracers, protocols, or scanners and sample size, may have contributed to not finding a correlation in this study. Future studies to advance knowledge with regard to tracer-specific uptake versus retention could encompass

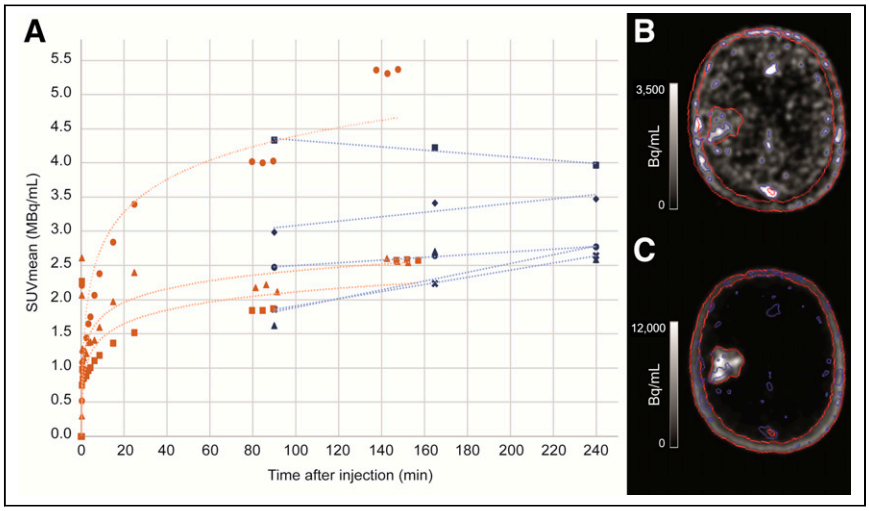

FIGURE 2. (A) Time–activity curves showing tumor uptake of [^{18}F]DCFpyl (orange) and [^{68}Ga]Ga-PSMA (blue) in MBq/mL from 0 to 240 min after injection for patients 1–8 (each marker icon represents one patient). Representative images of early (B, blue contour) and late (C, red contour) perfusion in first 2 min after injection of [^{18}F]DCFpyl in patient 6.

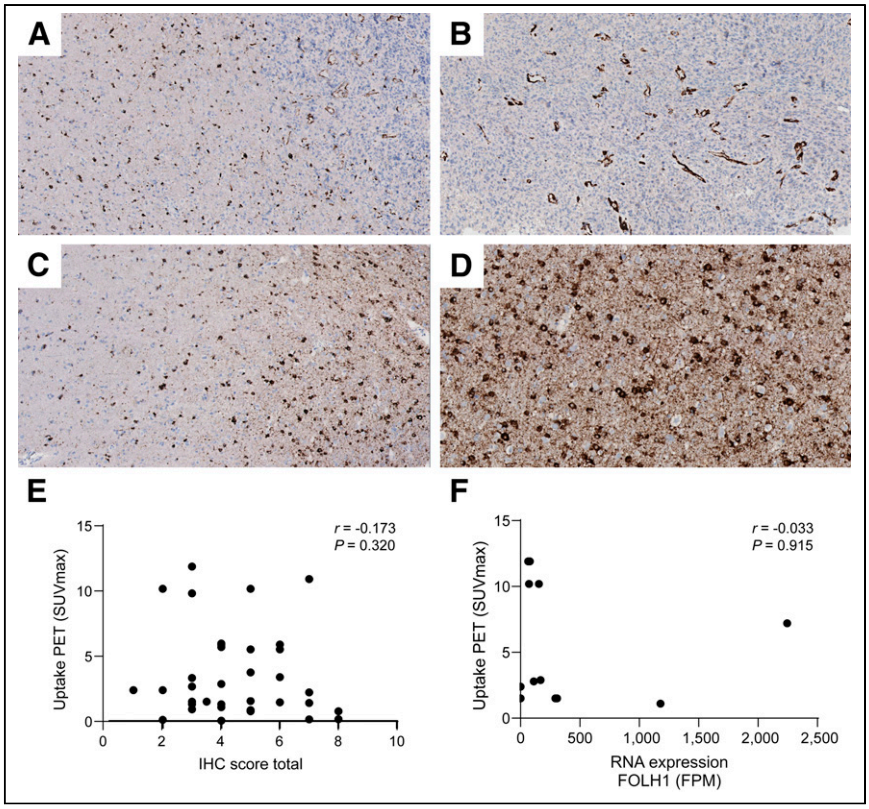

FIGURE 3. Representative images of PSMA immunohistochemistry in formalin-fixed and paraffin-embedded biopsy samples. (A) Positive, dispersed individual cells of unknown origin in periphery of tumor and positive vasculature in tumor cell–dense region. (B) Positive vasculature in tumor cell–dense region. (C) Positive, dispersed individual cells and granular staining in neuropil. (D) Positive individual cells and strong granular staining in neuropil. To exemplify method used for scoring IHC findings, following scores would have been given for these snapshot figures for microvasculature, individual cells, and granular staining in neuropil (sum score), respectively: 2, 3, and 1 (sum, 6) (A); 4, 0, and 0 (sum, 4) (B); 0, 3, and 3 (sum, 6) (C); and 0, 4, and 4 (sum, 8) (D). (E) Correlation between total IHC score and tracer uptake. (F) Correlation between normalized RNA expression of *FOLH1* (PSMA-encoding gene) and tracer uptake. Tracer uptake is expressed in SUV_{max} and measured on PET in 1-cm spheric volumes of interest in region on scan where biopsies were performed. IHC = immunohistochemistry; FOLH1 = folate hydrolase 1; FPM = fragments per million.

spatial transcriptomics or proteomics to study tracer heterogeneity within tumor or the tumor microenvironment at a cellular level. PET studies using radionuclides with long half-lives, such as ^{89}Zr, would enable in vivo quantitative uptake kinetics up to late time points. Animal models of GBM could be used to dynamically assess PSMA tracer uptake (by in vitro immunofluorescence) and combine this with ex vivo autoradiography, such as performed by Lindemann et al. (*30*). Competition experiments, such as with the PSMA inhibitor 2-phosphonomethyl pentanedioic acid, can be used to assess specific PSMA receptor binding on tumor neovasculature or cells (*32*).

In the clinical setting, for most studies on PSMA imaging in patients with GBM, PET scans have been acquired 60 min after injection of [^{68}Ga]Ga-PSMA-11 (*18,20,27,28*). Our composed time–activity curve implies that tumor-to-background ratios likely increase up to 240 min after injection for [^{68}Ga]Ga-PSMA-11. However, semiquantitative measures cannot be compared between scans acquired at different time points after injection of different tracers, because equilibrium kinetics vary and have not yet been reached within 240 min after injection.

In nonaffected brain tissue, we observed very low uptake of tracer, leading to high tumor-to-background ratios. In parotid tissue, expected high uptake of all PSMA tracers was observed, indicating this is the organ at risk for radionuclide therapy. Uptake in liver was comparable between patients, as previously reported (*26*), indicating that the liver is the most favorable organ to use as reference tissue for normalization of tracer uptake in tumor, although this does require whole-body scanning and thus more time.

This study has some limitations. The data originated from different centers that used different tracers, varying PET acquisition protocols, and reconstruction methods. We limited the influence of decay by choosing time points within the closest range from each of the centers for the SUV measurements at the biopsy locations (i.e., 120, 145, and 160 min after injection), and we chose those time points for which the time–activity curves showed a near-plateau phase of tracer uptake. Second, it is well known that the PET reconstruction method can influence the outcome of SUV measurements (*40,41*), and these differed across centers. Therefore, we also performed correlational analyses per tracer or center. The image analyses and immunohistochemistry scoring were uniformly performed to prevent additional variabilities because of data processing differences among the centers. Moreover, we think that the heterogeneity of the data represents the real-life clinical setting and gives important information on the comparability of the PSMA-targeting tracers for GBM imaging.

CONCLUSION

The observation in this study that various PSMA-targeting tracers show moderate to high uptake in GBM is hopeful and warrants further research into the exact mechanisms of PSMA accumulation or retention. Studies are needed to determine the actual potential of PSMA-targeted radionuclide therapy as an option for patients with GBM.

DISCLOSURE

Ilanah Pruis and Sophie Veldhuijzen van Zanten were financially supported by the Semmy Foundation. Marion Smits received speaker honoraria from Auntminnie and GE Healthcare and consultancy fees from Bracco. Daniela Oprea-Lager reports unrestricted grants from Janssen for consensus meeting attendance. Frederik Verburg received speaker honoraria from Sanofi, AstraZeneca, and Bayer and is a consultant to GE Healthcare. James Nagarajah received research support, consulting fees, and speaker fees from AAA/Novartis, POINT Biopharma, ABX, Curium, Bayer, Telix, and Sanofi. William Leenders is a shareholder and part-time employee at Radboudumc spin-off Predica Diagnostics. No other potential conflict of interest relevant to this article was reported.

ACKNOWLEDGMENTS

We thank Sandra Bossmann and Fleur Brienen for their help in patient inclusion, Benno Kusters for immunohistochemistry analyses,

and Marcel Segbers and Vera van Dis for their contribution to data acquisition and analysis.

KEY POINTS

QUESTION: What is the correlation between tumor uptake of PSMA-targeting tracers and PSMA expression in image-guided tumor biopsies in patients with de novo or recurrent GBM?

PERTINENT FINDINGS: In a multicenter inventory study in 14 GBM patients using [^{68}Ga]Ga-PSMA-11 ($n = 7$), [^{18}F]DCFPyl ($n = 3$), or [^{18}F]PSMA-1007 ($n = 4$) PET imaging, heterogeneous and significant uptake in tumor was found. PSMA expression was found on endothelial cells of tumor microvasculature, dispersed individual cells (of unknown origin), and granular staining of the neuropil, but no significant correlation was found between in vivo tracer uptake and PSMA expression levels.

IMPLICATIONS FOR PATIENT CARE: Various PSMA-targeting tracers show uptake in GBM, and further research into the exact mechanisms of PSMA accumulation or retention is warranted.

REFERENCES

1. Van de Wiele C, Sathekge M, de Spiegeleer B, et al. PSMA expression on neovasculature of solid tumors. *Histol Histopathol.* 2020;35:919–927.
2. Tanjore Ramanathan J, Lehtipuro S, Sihto H, et al. Prostate-specific membrane antigen expression in the vasculature of primary lung carcinomas associates with faster metastatic dissemination to the brain. *J Cell Mol Med.* 2020;24:6916–6927.
3. Traub-Weidinger T, Poetsch N, Woehrer A, et al. PSMA expression in 122 treatment naive glioma patients related to tumor metabolism in ^{11}C-methionine PET and survival. *J Pers Med.* 2021;11:624.
4. Wernicke AG, Edgar MA, Lavi E, et al. Prostate-specific membrane antigen as a potential novel vascular target for treatment of glioblastoma multiforme. *Arch Pathol Lab Med.* 2011;135:1486–1489.
5. Saffar H, Noohi M, Tavangar SM, Saffar H, Azimi S. Expression of prostate-specific membrane antigen (PSMA) in brain glioma and its correlation with tumor grade. *Iran J Pathol.* 2018;13:45–53.
6. Nomura N, Pastorino S, Jiang P, et al. Prostate specific membrane antigen (PSMA) expression in primary gliomas and breast cancer brain metastases. *Cancer Cell Int.* 2014;14:26.
7. Matsuda M, Ishikawa E, Yamamoto T, et al. Potential use of prostate specific membrane antigen (PSMA) for detecting the tumor neovasculature of brain tumors by PET imaging with ^{89}Zr-Df-IAB2M anti-PSMA minibody. *J Neurooncol.* 2018;138:581–589.
8. Holzgreve A, Biczok A, Ruf VC, et al. PSMA expression in glioblastoma as a basis for theranostic approaches: a retrospective, correlational panel study including immunohistochemistry, clinical parameters and PET imaging. *Front Oncol.* 2021;11:646387.
9. Gao Y, Zheng H, Li L, et al. Prostate-specific membrane antigen (PSMA) promotes angiogenesis of glioblastoma through interacting with ITGB4 and regulating NF-κB signaling pathway. *Front Cell Dev Biol.* 2021;9:598377.
10. Mahzouni P, Shavakhi M. Prostate-specific membrane antigen expression in neovasculature of glioblastoma multiforme. *Adv Biomed Res.* 2019;8:18.
11. Salas Fragomeni RA, Menke JR, Holdhoff M, et al. Prostate-specific membrane antigen-targeted imaging with [^{18}F]DCFPyL in high-grade gliomas. *Clin Nucl Med.* 2017;42:e433–e435.
12. Schwenck J, Tabatabai G, Skardelly M, et al. In vivo visualization of prostate-specific membrane antigen in glioblastoma. *Eur J Nucl Med Mol Imaging.* 2015;42:170–171.
13. Tanjore Ramanathan J, Lehtipuro S, Sihto H, et al. Prostate-specific membrane antigen expression in the vasculature of primary lung carcinomas associates with faster metastatic dissemination to the brain. *J Cell Mol Med.* 2020;24:6916–6927.
14. Haberkorn U, Eder M, Kopka K, Babich JW, Eisenhut M. New strategies in prostate cancer: prostate-specific membrane antigen (PSMA) ligands for diagnosis and therapy. *Clin Cancer Res.* 2016;22:9–15.
15. Bertagna F, Albano D, Cerudelli E, Gazzilli M, Giubbini R, Treglia G. Potential of radiolabeled PSMA PET/CT or PET/MRI diagnostic procedures in gliomas/glioblastomas. *Curr Radiopharm.* 2020;13:94–98.
16. Pilati E, Nicolotti DG, Ceci F, et al. ^{68}Ga-prostate-specific membrane antigen 11 PET/CT detects residual glioblastoma after radical surgery in a patient with synchronous recurrent prostate cancer: a case report. *Clin Nucl Med.* 2020;45:e151–e153.
17. Gupta M, Choudhury PS, Premsagar IC, Gairola M, Ahlawat P. Role of ^{68}Ga-prostate-specific membrane antigen PET/CT in disease assessment in glioblastoma within 48 hours of surgery. *Clin Nucl Med.* 2020;45:204–205.
18. Kumar A, ArunRaj ST, Bhullar K, et al. Ga-68 PSMA PET/CT in recurrent high-grade gliomas: evaluating PSMA expression in vivo. *Neuroradiology.* 2022;64:969–979.
19. Jiang JY, Kang C, Bui P, Mansberg R. Incidental prostate-specific membrane antigen-avid glioblastoma detected on ^{68}Ga-prostate-specific membrane antigen PET/CT. *Radiol Case Rep.* 2022;17:2023–2025.
20. Kunikowska J, Kulinski R, Muylle K, Koziara H, Krolicki L. ^{68}Ga-prostate-specific membrane antigen-11 PET/CT: a new imaging option for recurrent glioblastoma multiforme? *Clin Nucl Med.* 2020;45:11–18.
21. Truckenmueller P, Graef J, Scheel M, et al. [^{68}Ga]Ga-PSMA PET/MRI, histological PSMA expression and preliminary experience with [^{177}Lu]Lu-PSMA therapy in relapsing high-grade glioma. *Front Oncol.* 2022;12:980058.
22. Giraudet AL, Kryza D, Hofman M, et al. PSMA targeting in metastatic castration-resistant prostate cancer: where are we and where are we going? *Ther Adv Med Oncol.* 2021;13:17588359211053898.
23. Kunikowska J, Charzyńska I, Kuliński R, Pawlak D, Maurin M, Królicki L. Tumor uptake in glioblastoma multiforme after IV injection of [^{177}Lu]Lu-PSMA-617. *Eur J Nucl Med Mol Imaging.* 2020;47:1605–1606.
24. Cranial navigation application. Brainlab website. https://www.brainlab.com/surgery-products/overview-neurosurgery-products/cranial-navigation/. Published 2022. Accessed July 18, 2023.
25. de Bitter T, van de Water C, van den Heuvel C, et al. Profiling of the metabolic transcriptome via single molecule molecular inversion probes. *Sci Rep.* 2017;7:11402.
26. Ferreira G, Iravani A, Hofman MS, Hicks RJ. Intra-individual comparison of ^{68}Ga-PSMA-11 and ^{18}F-DCFPyL normal-organ biodistribution. *Cancer Imaging.* 2019;19:23.
27. Sasikumar A, Joy A, Pillai MR, et al. Diagnostic value of ^{68}Ga PSMA-11 PET/CT imaging of brain tumors: preliminary analysis. *Clin Nucl Med.* 2017;42:e41–e48.
28. Sasikumar A, Kashyap R, Joy A, et al. Utility of ^{68}Ga-PSMA-11 PET/CT in imaging of glioma: a pilot study. *Clin Nucl Med.* 2018;43:e304–e309.
29. Verma P, Malhotra G, Goel A, et al. Differential uptake of ^{68}Ga-PSMA-HBED-CC (PSMA-11) in low-grade versus high-grade gliomas in treatment-naive patients. *Clin Nucl Med.* 2019;44:e318–e322.
30. Lindemann M, Oteiza A, Martin-Armas M, et al. Glioblastoma PET/MRI: kinetic investigation of [^{18}F]rhPSMA-7.3, [^{18}F]FET and [^{18}F]fluciclovine in an orthotopic mouse model of cancer. *Eur J Nucl Med Mol Imaging.* 2023;50:1183–1194.
31. Sácha P, Zámecník J, Barinka C, et al. Expression of glutamate carboxypeptidase II in human brain. *Neuroscience.* 2007;144:1361–1372.
32. Oliveira D, Stegmayr C, Heinzel A, et al. High uptake of ^{68}Ga-PSMA and ^{18}F-DCFPyL in the peritumoral area of rat gliomas due to activated astrocytes. *EJNMMI Res.* 2020;10:55.
33. Thompson SM, Suman G, Torbenson MS, et al. PSMA as a theranostic target in hepatocellular carcinoma: immunohistochemistry and ^{68}Ga-PSMA-11 PET using cyclotron-produced ^{68}Ga. *Hepatol Commun.* 2022;6:1172–1185.
34. Rüschoff JH, Ferraro DA, Muehlematter UJ, et al. What's behind ^{68}Ga-PSMA-11 uptake in primary prostate cancer PET? Investigation of histopathological parameters and immunohistochemical PSMA expression patterns. *Eur J Nucl Med Mol Imaging.* 2021;48:4042–4053.
35. Ferraro DA, Rüschoff JH, Muehlematter UJ, et al. Immunohistochemical PSMA expression patterns of primary prostate cancer tissue are associated with the detection rate of biochemical recurrence with ^{68}Ga-PSMA-11-PET. *Theranostics.* 2020;10:6082–6094.
36. Stockhammer F, Plotkin M, Amthauer H, van Landeghem FK, Woiciechowsky C. Correlation of F-18-fluoro-ethyl-tyrosin uptake with vascular and cell density in non-contrast-enhancing gliomas. *J Neurooncol.* 2008;88:205–210.
37. Vettermann FJ, Diekmann C, Weidner L, et al. L-type amino acid transporter (LAT) 1 expression in ^{18}F-FET-negative gliomas. *EJNMMI Res.* 2021;11:124.
38. Lapa C, Linsenmann T, Lückerath K, et al. Tumor-associated macrophages in glioblastoma multiforme: a suitable target for somatostatin receptor-based imaging and therapy? *PLoS One.* 2015;10:e0122269.
39. Kiviniemi A, Gardberg M, Frantzén J, et al. Somatostatin receptor subtype 2 in high-grade gliomas: PET/CT with ^{68}Ga-DOTA-peptides, correlation to prognostic markers, and implications for targeted radiotherapy. *EJNMMI Res.* 2015;5:25.
40. Rogasch JMM, Hofheinz F, van Heek L, Voltin CA, Boellaard R, Kobe C. Influences on PET quantification and interpretation. *Diagnostics (Basel).* 2022;12:451.
41. Mansor S, Pfaehler E, Heijtel D, Lodge MA, Boellaard R, Yaqub M. Impact of PET/CT system, reconstruction protocol, data analysis method, and repositioning on PET/CT precision: an experimental evaluation using an oncology and brain phantom. *Med Phys.* 2017;44:6413–6424.